

New Computer System for Recognizing Micro- and Nano-Sized Objects in Semiconductors and Colloidal Solutions

L. Diachenko¹, E. Minov¹, S. Ostapov¹, P. Fochuk¹, Yu. Khalavka¹, A. Bolotnikov², R.B. James²

¹ Chernivtsi National University, Chernivtsi, Ukraine

² Brookhaven National Laboratory, Upton, New York, USA

(Received 15 September 2016; published online 23 December 2016)

In this paper it is describe a new approach developed for recognizing micro- and nano-sized objects and a method for quantitative analysis of these objects. For this purpose was developed the automated systems that can simplify and accelerate the process of nanoparticle tracks analysis under the microscope whereby engineers and scientists are able to recognize the structures of defects in semiconductor wafers, along with nanoparticles and other microscopic objects. This capability is important to both select appropriate crystals and also to apply the data to improve the production process.

Keywords: Optical defect recognition, Nano-tracking analysis, Computer vision, Growth defects, Software developing.

DOI: [10.21272/jnep.8\(4\(2\)\).04060](https://doi.org/10.21272/jnep.8(4(2)).04060)

PACS numbers: 07.05.Rm; 07.05.Tp

1. INTRODUCTION

Object recognition systems based on computer vision are used currently in various fields of science and industry. For instance, they are employed for studying the quality of building structures and the surface- and internal-structure of metal parts, PCB electronic equipment, and the manufacturing of fabrics [1-3]. They are especially useful in the semiconductor industry. The production of suitable semiconductor crystals is becoming more complex, as the growth and fabrication processes may encompass a few hundred precisely controlled steps. In the case of CdTe/CdZnTe (CZT) crystals, the main technological approach to eliminate, or at least, reduce the presence of inclusions in such crystals is by annealing them at high temperatures, often in a controlled Cd over-pressure [4-9]. Even short-term annealing can considerably reduce the size and concentration of inclusions (see Fig. 1) [10]. It is clear that the process of annealing must also be accurately controlled and monitored to assure a satisfactory removal of inclusions, since for this industry, the detrimental effects of extended defects, such as inclusions, is often the primary factor limiting device performance [11].

Usually, systems for imaging inclusions in CdTe operate on the basis of analyzing a stacked series of photographs obtained via infrared transmission through a microscope. The focused layer-by-layer images can be used to reveal the internal structure of the subsystem of crystalline defects. Thus, an experienced crystal grower can use the 3D distribution of defects and their statistical variations among different samples to refine the parameters of the growth process.

In practice, R&D investigations to improve the crystal growth often spend a large amount of time to understand the presence and cause of defects based on systematic variations in the growth parameters. In addition, the manual process of classifying all of the defects (for example, by size) is extremely laborious and time consuming. Furthermore, the challenge to vary a single growth parameter, while leaving all others fixed, poses many challenges, leading to errors in classifica-

tion, failures to properly identify the causes for defect formation, and an inability to determine correlations between growth parameters and material and device properties.

A similar problem confronts researchers seeking to measure nano-sized objects (e.g., in the case of tracking sub-micron particles in colloidal solutions). In this work we introduce a new method for nano-tracking analysis (NTA). It is a relatively simple method to analyze mono- and poly-dispersed mixtures of small particles (e.g., polystyrene nanoparticles in liquid crystals and submicron protein aggregations in human blood serum and plasma for studying biosystems of exosomes). These nanoparticles are cellular vesicles 30-100 nm in size, which constitute potential means for drug delivery in protein and RNA treatment [12-15]. With NTA, we also can measure the parameters of suspensions, for example, to determine the local temperature and viscosity of the solution with an accuracy of better than 2.5 %. Analysis of nanoparticle tracks under the microscope cannot be done manually, and hence, this process requires automation.

Accordingly, it is vital to develop automated systems that can simplify and accelerate the process whereby engineers and scientists are able to recognize the structures of defects in semiconductor wafers, along with nanoparticles and other microscopic objects. This capability is important to both select appropriate crystals and also to apply the data to improve the production process.

To verify the reliability of recognition systems for measuring microscopic defects, we need to have accurate information about their presence in the crystal, including their size and spatial distribution. But accurate knowledge regarding the steps to strictly control the specific growth parameters related to each defect subsystem is unknown as yet.

One of the solutions of this problem is to verify a recognition process by means of a "virtual" crystal, generated by a computer program. This method allows our setting of the desired number of various defects and their positions in the "virtual" crystal according to a

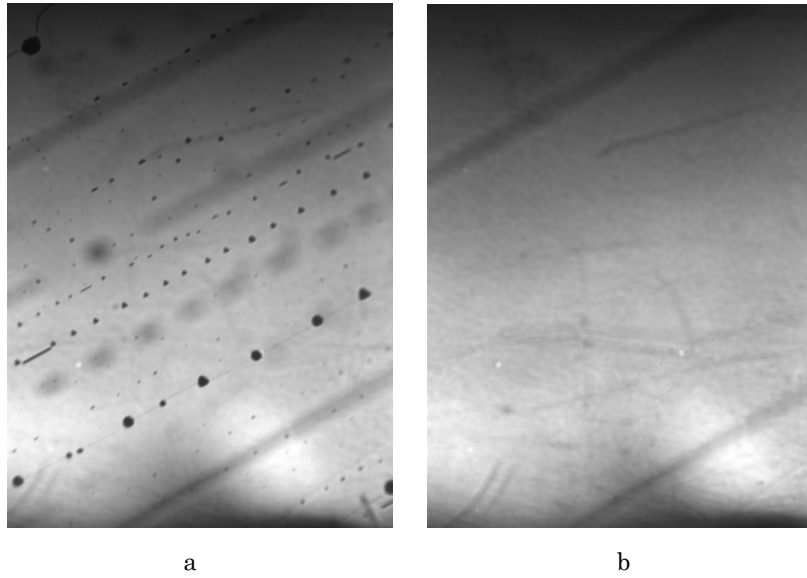


Fig. 1 – IR transmission images of CZT samples annealed at 1100 K under Cd overpressure for 60 minutes. Photo, shows an as-grown sample (a), Photo, shows same region after thermal treatment (b). The size of the image is $0.9 \times 0.6 \text{ mm}^2$

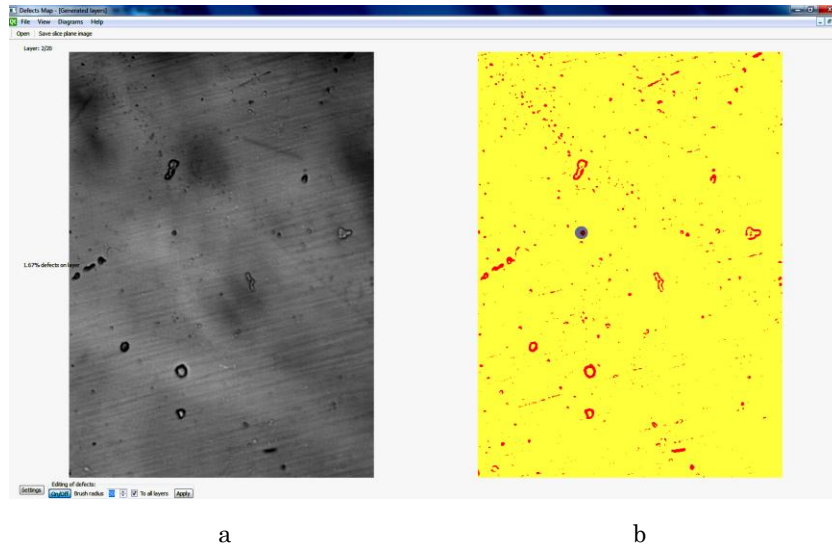


Fig. 2 – Infrared transmission image of a semiconductor crystal (Dark grey region: defects in the crystal) (a), Recognition results based on the infrared image (Red features are defects in the crystal, and grey is used for editing, in this case for deleting selected defects.) (b)

specified statistical distribution. The software generates a set of layered photographs of such a "crystal" and a file with the statistics describing the defect subsystem. A set of photographs is input to the recognition software, and the results obtained after statistical analysis are compared with the input. Thus, we get quantitative criteria on the quality of the defects-recognition program and can compare for different analysis programs.

The main purpose of this paper is to describe a new approach developed for recognizing micro- and nano-sized objects and a method for quantitative analysis of these objects.

2. RECOGNITION METHOD

The first step in the analysis process is the pre-filtration of the input image based upon a set number

of decomposition levels of discrete orthogonal wavelet-transformation [16-17]. The goal is to smooth the high-frequency noise surrounding the defects. The number of decomposition levels depends on the size of the input image. Each element of the wavelet transformation (2.1) and wavelet synthesis (2.2) is given by the following equations:

$$DWT(M^{in}, N_x, N_y, d) = \begin{cases} DWT_{XY}(M^{in}, N_x, N_y), & d < 1, \\ DWT(DWT_{XY}(M^{in}, N_x, N_y), \frac{N_x}{2}, \frac{N_y}{2}, d-1), & d \geq 1. \end{cases} \quad (2.1)$$

$$DWT^{-1}(M^{in}, N_x, N_y, d) = \begin{cases} DWT_{XY}^{-1}(M^{in}, N_x, N_y), & d < 1, \\ DWT^{-1}(DWT_{XY}^{-1}(M^{in}, N_x, N_y), \frac{N_x}{2}, \frac{N_y}{2}, d-1), & d \geq 1. \end{cases} \quad (2.2)$$

Here, M^{in} is the input matrix of the image; N_x and N_y are the image's width and height; and DWT and DWT^{-1} are the wavelet transformation and wavelet

synthesis, respectively. The application of filters can be described by the following equations:

$$W_F(M^{in}, S, d) = \begin{cases} \begin{cases} M_{x,y}^{in}, & d < 1, \\ W_F(M^{in}, S \times 0.5, d-1)_{x,y}, & d \geq 1. \end{cases} & \left(x < \frac{w \times S}{2}\right) \& \left(y < \frac{h \times S}{2}\right), \\ \begin{cases} M_{x,y}^{in}, & M_{x,y}^{in} \geq W_{TR} \\ W_S \times M_{x,y}^{in}, & M_{x,y}^{in} < W_{TR} \end{cases}, & else. \end{cases}$$

$$W_{x,y}^L = DWT^{-1}\left(W_F(DWT(M^{in}, w, h, d), d), w, h, d\right)_{x,y}.$$

Here, w and h are the image's width and height; S is the image's scale factor; d is the number of decomposition levels (4-7 are typically enough depending on the image's size); W_F is the function for filtering the high-frequency component; W_{TR} is the filtering threshold; and $W_{x,y}^L$ is the matrix of the filtered image.

The second stage is the recognition of defects, where the results thereof are denoted in bit fields, each element of which is given by the formulae below:

$$B_{x,y}^F = \begin{cases} 1, & R_{x,y}^M \geq R_{TR}, \\ 0, & R_{x,y}^M < R_{TR}, \end{cases}$$

$$R_{x,y}^M = W_{x,y}^L - R_{x,y}^{Blur},$$

$$FB_{x,y}^F = \frac{1}{(2F_{Rad})^2} \begin{cases} \sum_{u=0}^{2F_{Rad}} \sum_{v=0}^{2F_{Rad}} B_{(x+u)-F_{Rad}, (y+v)-F_{Rad}}^F, & B_{(x+u)-F_{Rad}, (y+v)-F_{Rad}}^F > 0 \\ 0, & B_{(x+u)-F_{Rad}, (y+v)-F_{Rad}}^F \leq 0. \end{cases}$$

The fourth stage is sorting the defects by area in the filtered bit-field. During this work, the sorting algorithm generates defects and fills the matrix indices, each of which corresponds to the position of the defect in the bit field, and also indicates the group to which each particular defect belongs.

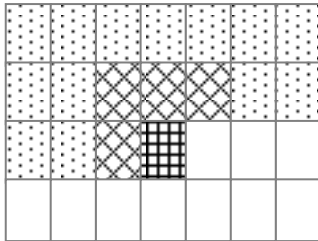


Fig. 3 – Mask for grouping of defects per pixel. Current pixel, processed pixel, and is one of the four adjacent previously-processed pixels to which the current pixel is compared. The blank pixels are not revealed at the step that is depicted

The next stage is the process of image segmentation. After receiving the recognized bit field, image segmentation is undertaken. The grouping of the defect

$$R_{x,y}^{Blur} = \frac{1}{(2R_{Rad})^2} \sum_{u=0}^{2R_{Rad}} \sum_{v=0}^{2R_{Rad}} W_{(x+u)-R_{Rad}, (y+v)-R_{Rad}}^L.$$

Here, R_{TR} is the recognition threshold; $B_{x,y}^F$ is the bit field, the matrix (internal representation of the image); $R_{x,y}^{Blur}$ is the matrix of the blurred image; and R_{Rad} is the recognition radius.

The third stage is the filtering of the bit field, where the goal is to sift out large areas with small defects. The algorithm works by analyzing neighboring pixels. Each element of the filtered bit field is given by the following Eq.:

pixels (i.e., segmentation) for each layer is performed via a per-pixel review of each layer's bit field, and by comparing each pixel with the four pixels already analyzed that are positioned around the particular one at issue (see Fig. 3).

The result of segmentation is the localization of objects that further is used for creating a three-dimensional model of the subsystem of crystal defects or for nano-tracking.

The input data for tracking nanoparticles also can be displayed as video files, typically in *avi*-format. In this case, we use the fact that nanoparticles possessing different nature (e.g., shape) scatter light differently; in addition, the dispersed light from their images often differs in color. Therefore, the choice of a color filter can help to discriminate different types of particles. Considering this observation, data obtained by NTA also can be used to identify nanoparticles of different nature, as well as to classify their characteristics according to strongly anisotropic shapes, such as rods, tubes, and plates.

For investigations that require tracking of nanoparticles, we can use Eq. (2.3) to calculate the values of velocity and the arithmetic mean of the squared dis-

placement for each track step through the use of our recognition system and video record.

$$MSD = \frac{1}{4N} \times \sum_{n=1}^N \sqrt{((p_{x_n} - p_{x_{n-1}})P_S)^2 + ((p_{y_n} - p_{y_{n-1}})P_S)^2}. \quad (2.3)$$

Here, N is the number of motion frames of the nanoparticles; n is index of the current track frame; p_x is nanoparticles' track position on the axis x ; p_y is nanoparticles' track position on the axis y ; and P_S is the pixel size in millimeters.

If an object disappears from one video frame and appears in another one, the system analyzes the points of both the disappearance and reappearance, and if necessary, joins these tracks into a single one using remote detection and time-thresholds settings.

Knowing the size of the nano-objects, one can use nano-tracking to determine different solution parameters, such as local temperature and viscosity.

In the "classic" algorithm for determining size, the diameter of the nanoparticles is given by the Stokes-Einstein formula:

$$d = \frac{TK_B t}{3\pi \frac{\eta}{1000} MSD}.$$

Where the viscosity and temperature is given by:

$$\eta = \frac{TK_B t}{3\pi d MSD} \times 1000; \quad (2.4)$$

$$T = \frac{3\pi d \frac{\eta}{1000} MSD}{K_B t}. \quad (2.5)$$

Here, T is the solution temperature in units of Kelvin; K_B is the Boltzmann constant; t is the time (frames per second); d is the average diameter of the objects; and η is the solution's viscosity coefficient.

The model described above is used to guide the software development for analyzing the defect subsystems in solids, and also for nano-tracking.

3. SOFTWARE DESCRIPTION

We developed custom software to perform the assigned tasks. We used C++ MinGW Toolchain (GCC 3.4.5), Qt SDK Win and Matlab 7.11.0.584 (R2010b) Opensource Frameworks, and Qt Creator for IDE construction. One part of the developed software is a program for recognition and modeling the three-dimensional structure of a defect subsystem in a semiconductor crystal – *DefectMap*; another part is the system for the "virtual" crystal generation, *DefectGen*. Figure 4 shows a block diagram of the developed software.

Such modeling is performed by analyzing a series of crystal photos obtained using infrared transmitted light via a microscope. The microscope scans the crystal, layer by layer at different depths, adjusting the optics to sharpen the focus at each depth. Photos recorded in the correct order constitute the input of the

recognition software, which is represented in *jpg* format. First, the program detects growing defects in each picture separately, and then builds a three-dimensional image of the defect subsystems.

DefectMap provides tools for editing the recognized images. We can remove the defects on the crystal's surface caused by damage during surface processing, as well as regions in the photos that were wrongly recognized as defects. If any changes were made in the recognized images, they can be applied to the current layer or to other layers, including those constituting a three-dimensional image. For example, Figure 2 presents the results of infrared image recognition and demonstrates the usage of editing. Figure 5 presents a three-dimensional model of the subsystem of crystal defects built from the photos.

This model can be arbitrarily rotated using a mouse, so that it can display a specific group of defects and its distribution. By default, defects are divided into different sub-groups, for example, less than 5-microns diameter (blue points on 3D image in Fig. 5.a), 5-20 microns (green defects on 3D image in Fig. 5.a), and, more than 20 microns (red defects on 3D image in Fig. 5.a).

One issue to be addressed is the reliability of the recognition software, because we cannot grow a crystal with predetermined parameters for a defect subsystem, since the formation of the defects is a statistical effect with a highly complex distribution.

Since we cannot grow such crystals, computer technology is used to generate "virtual" crystals with known parameters related to the growth process. The crystal can be "cut" into "virtual layers", and a set of photos can be created for the recognition program. The difference of this set to others is that it can reflect statistical variations used as inputs to the program, which will include the number of growing defects in each group (e.g., small – less than 5 micron diameter; average – from 5 to 20 microns; and large – greater than 20 microns). It can also include linear- and planar-shaped defects, the statistical distribution of each class of defect within each layer, and the overall 3D distribution for the full crystal.

This set of photos (in *jpg* format) can be sent as input to the recognition software, which will recognize it and compare the results with the input statistics. Such an approach not only will allow us to quantitatively analyze the quality of such programs, but to also compare the output using different recognition software.

DefectGen is the program used to generate such a "virtual" crystal together with the statistics file. When generating "virtual defects", the spheres' radii are used, and their coordinates are randomly set in a three-dimensional crystal. The distribution of statistical can be chosen from the following ones: Poisson, Gaussian, homogeneous (Box - Muller transform), or random function.

The z coordinate is used to divide the "virtual" crystal into different layers. In the process of generating the bit field of each layer, we obtain the reflection of generated defects for this plane. For each defect-sphere, the distance to the current layer is calculated via the z coordinate with subsequent pruning of the defect's radius and the depth of sharpness for the layers:

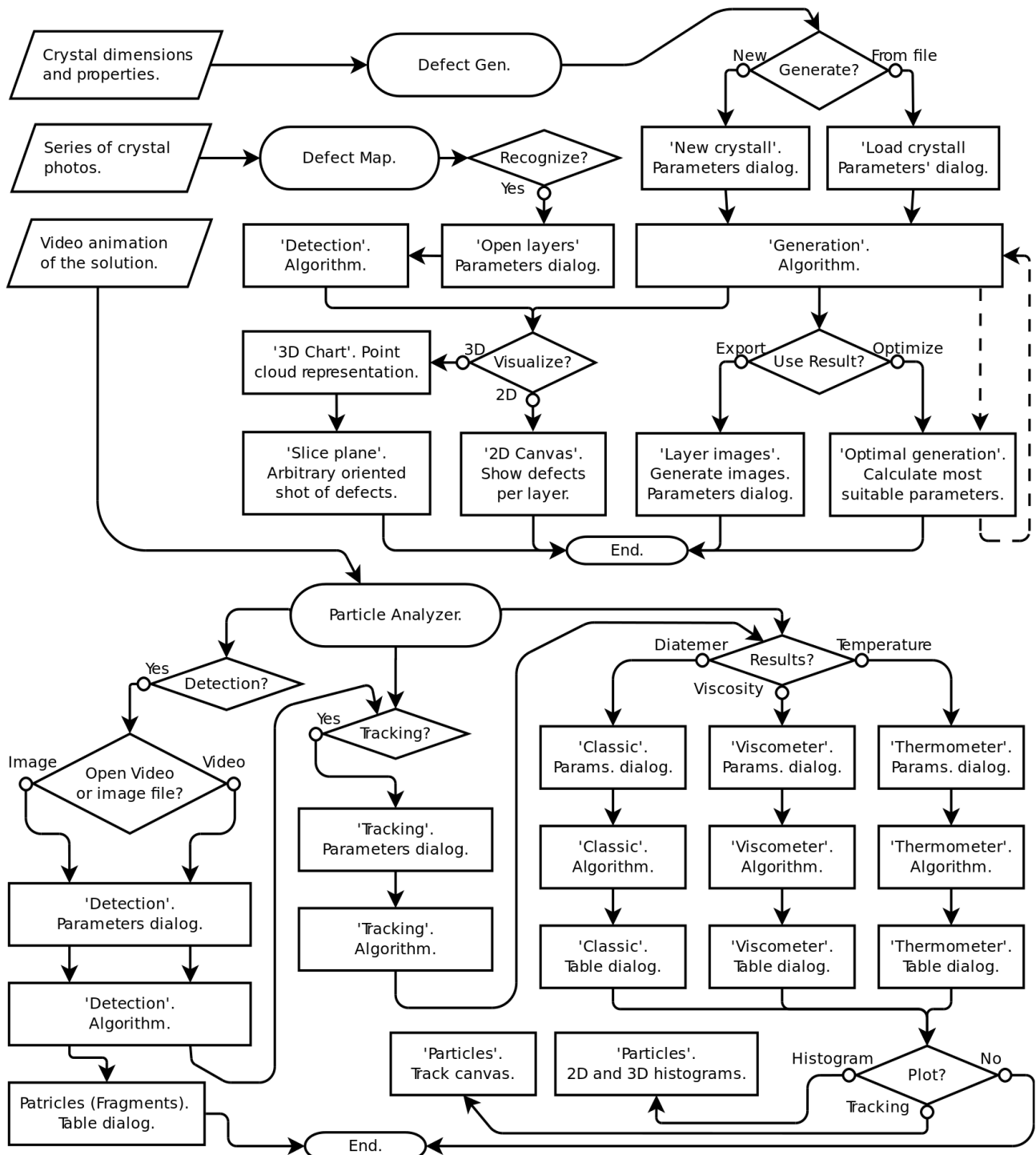


Fig. 4 – Block diagram for our recognition system for micro- and nano-sized objects

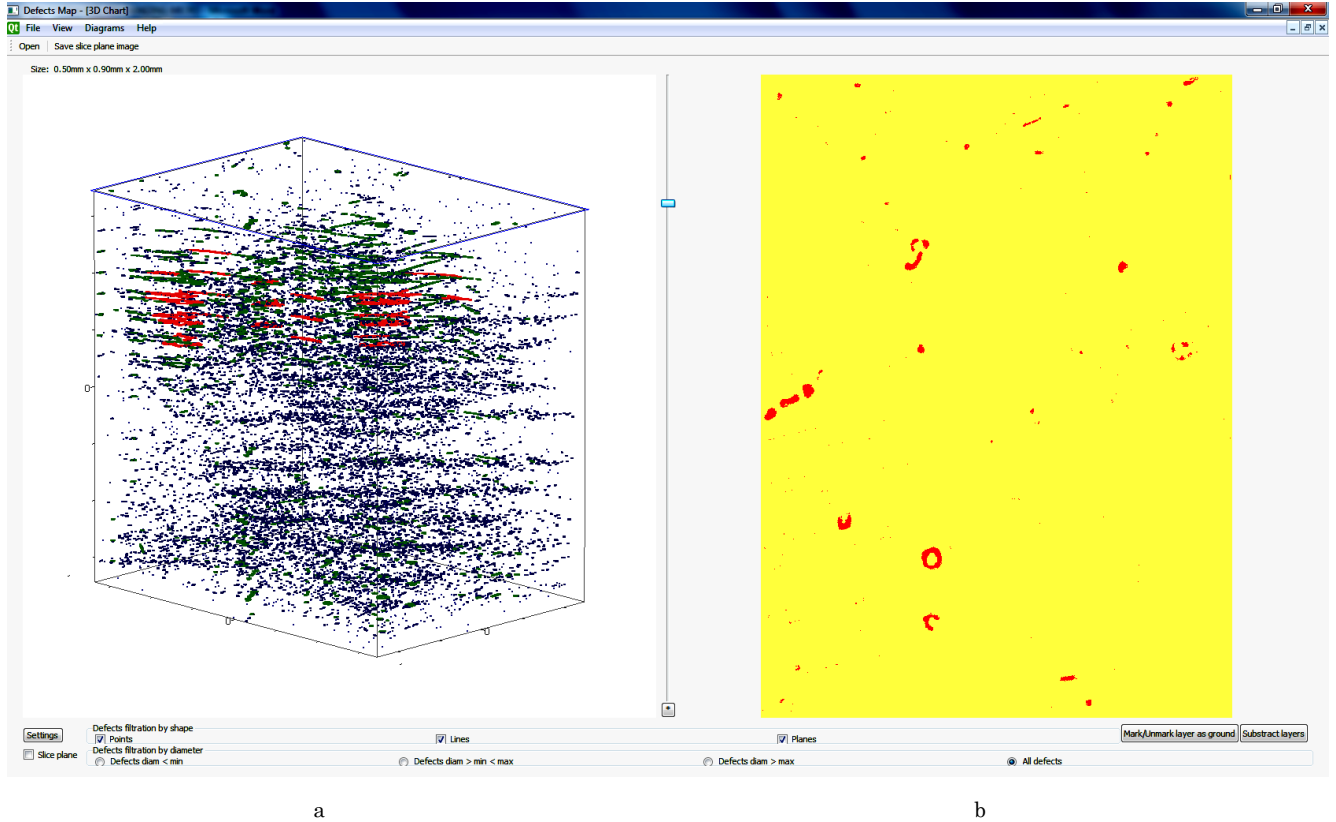


Fig. 5 – Three-dimensional image of the crystal (a), Recognition result of one of the layers in the 3D image (in this case it is the first layer used to form the 3D image shown on the left) (b). The user can select any layer from the 3D image for representation on the right panel

$$\Delta_Z = \left| Z^{def} - Z^{lay} \right| - \frac{D^{lay}}{2},$$

$$\Delta_Z = \begin{cases} 0, & \Delta_Z < 0, \\ \Delta_Z, & \Delta_Z \geq 0. \end{cases}$$

$$\Delta = \left\{ X^{def} - X^{lay}, Y^{def} - Y^{lay}, \Delta_Z \right\}.$$

Here, Δ_Z is the distance from the defect center to the layer; Z^{def} is the defect z coordinate; Z^{lay} is the layer's z coordinate in the crystal's reference system; and D^{lay} is the recognition depth of optimal sharpness.

The pruning condition for the current layer is the following: $\Delta_Z \geq R^{def}$. Based on the designated distance, the bit-field for the layers is given by:

$$\sum_{n=1}^N \sum_{x,y,z=0}^{N_{x,y,z}} F_{X,Y,Z}^{Pix} = \begin{cases} 1, & |\Delta_{N,XYZ}| < R^{def} \\ 0, & else \end{cases}$$

Where N is the number of standard defects, N_z represents the number of layers, and N_x and N_y are, accordingly, the layer's width and length.

After processing each layer's bit-field, the program generates the set of photos and builds a three-dimensional image of a crystal, as in the case of *DefectMap*. Simultaneously, it generates statistical information about the defect subsystem of the "virtual" crystal. The set of pictures and the description file then are saved to a disk.

For convenience in analyzing the defect subsystem, the software supports an arbitrary cross-section of the "virtual" crystal; moreover, the surface of the cutting plane surface can be moved and rotated arbitrarily. Each selected cross-section image can be saved to disk.

There is the possibility of obtaining "noisy" pictures with different distributions, and the intensity of the noise changes the contrast, brightness, and image details.

Accordingly, the program for generating "virtual" crystals is a good method for checking the recognition software. After we obtained the set of photos of the needed distribution of the quantity and size of defects, we can check the accuracy of the recognition programs in the defect recognition, along with the type or size of defects that were not detected properly (for example, the program poorly recognizes small defects, planes, and low levels of noise).

A slight modification of the programs described above allows us to apply them for analyzing the tracks of metal nanoparticles in colloid solutions. The video file recorded by a camera used with the microscope serves as the input data. A 30-second video is adequate for analysis.

Before beginning the nano-tracking process, the detection and tracking parameters can be optimized for the best tracking results.

Here, the radius for a particle search can be configured, and the components of one particle track can be searched on different frames, on a minimum length of track, and with time- and distance-thresholds, by

which the obtained settings will be filtered. Since the calculations by the NTA method are based on real pixel size, the optical parameters must be configured for the type of microscope and cameras (e.g., optical, digital zoom, and so on).

For calculating the diameter of nanoparticles, one should also set the values for the temperature and viscosity of the solution, along with the range of particle diameters. This will help to prevent distortion of the

statistics if noise or another object appears in the video.

In modes of micro-viscometer and micro-thermometer, solution viscosity and temperature are calculated by formulas (2.4)-(2.5), and also the type of algorithm that will be used is chosen.

The results of the calculation are displayed in the data table from which 2- and 3-dimensional image histograms and the track image of the selected particle can be obtained (Figure 6).

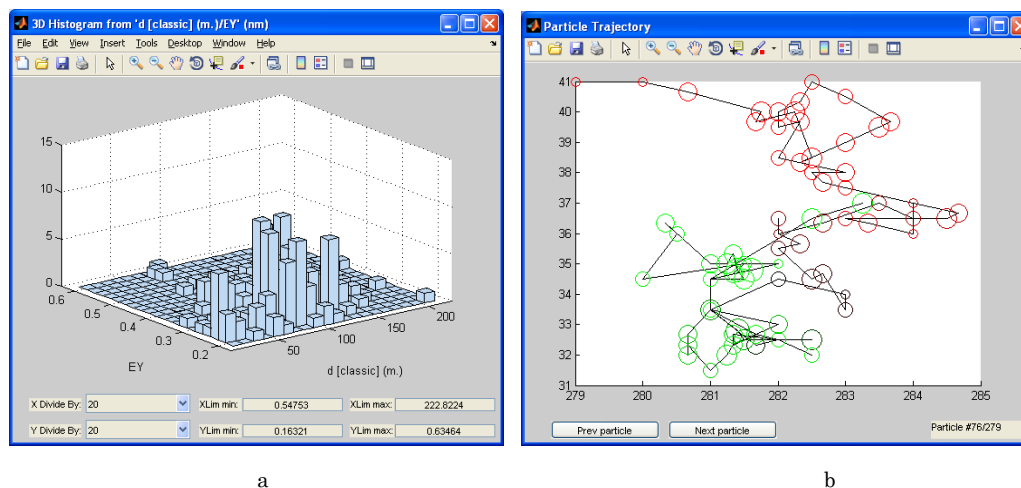


Fig. 6 – Nanoparticle distribution (a) and tracking results (b)

Thus, the developed software gives researchers the opportunity to automate the process of nano-tracking, and it can be used as a tool for research into the parameters and behavior of nanoparticles in solutions. The system also can be also used in the modes of micro-viscometry and micro-thermometry to measure the solution's parameters.

4. SOFTWARE TESTING

This section presents the results from testing the developed software, especially *DefectGen* and *DefectMap*. The basic settings of both programs are as follows:

- Number of layers – 20;
- Sharpness depth – 10 μm ;
- Minimal diameter of defect – 5 μm ;
- Maximal diameter of defect – 20 μm ;

In all cases, testing was performed as follows: The *DefectGen* program created a "virtual" crystal with pre-determined parameters, and a photograph set (20 items) was generated. This set was sent to the *DefectMap* program for object recognition. The recognition results were compared to the statistics file of the "virtual" crystal, and the correctness of the recognition process was determined.

4.1 Test 1

The recognition correctness for only big defects. A "virtual" crystal with 20 big defects with sizes over 20 μm was generated, without any additional noise in the photos. The results of the recognition are shown in Fig. 7.

The histograms demonstrate that most of the detected defects are larger than 20 μm . *DefectMap* recognized 18 of 20 defects larger than 20 μm (green color). It also recognized several medium- and small-sized

defects (yellow and red colors respectively), which were filtered out as noise. The degree of accuracy of the recognition for big defects (90 %) is very good. Similar results were obtained in other simple tests with several other types and numbers of defects.

4.2 Test 2

The correctness of recognition of big defects with noise included. To further the testing, we put 5% noise onto the photos. After analyzing the photos, *DefectMap* recognized the total number of large defects, i.e., 20. Furthermore, we obtained 72 small defects. The imposed noise was the reason for the recognition of the small defects, because it was not filtered out.

4.3 Test 3

Recognition correctness for medium-sized defects. A "virtual" crystal was generated with 300 average-sized defects (5-20- μm diameter) without any additional noise added to the photos. In the histogram of the distribution of the detected defects, it is evident that most of medium-sized defects are seen. Overall 290 from the total of 300 such defects were recognized. In addition, 6 small defects (less than 5- μm diameter) were detected.

4.4 Test 4

The correctness of the medium-sized defects recognition when noise is added. We added 5% noise to the previous case. Analysis of the recognition histogram revealed that the average number of defects is approximately the same as in the previous case (287 instead of 290), but the number of small defects increased from 6 to 80 due to the inclusion of 5 % noise.

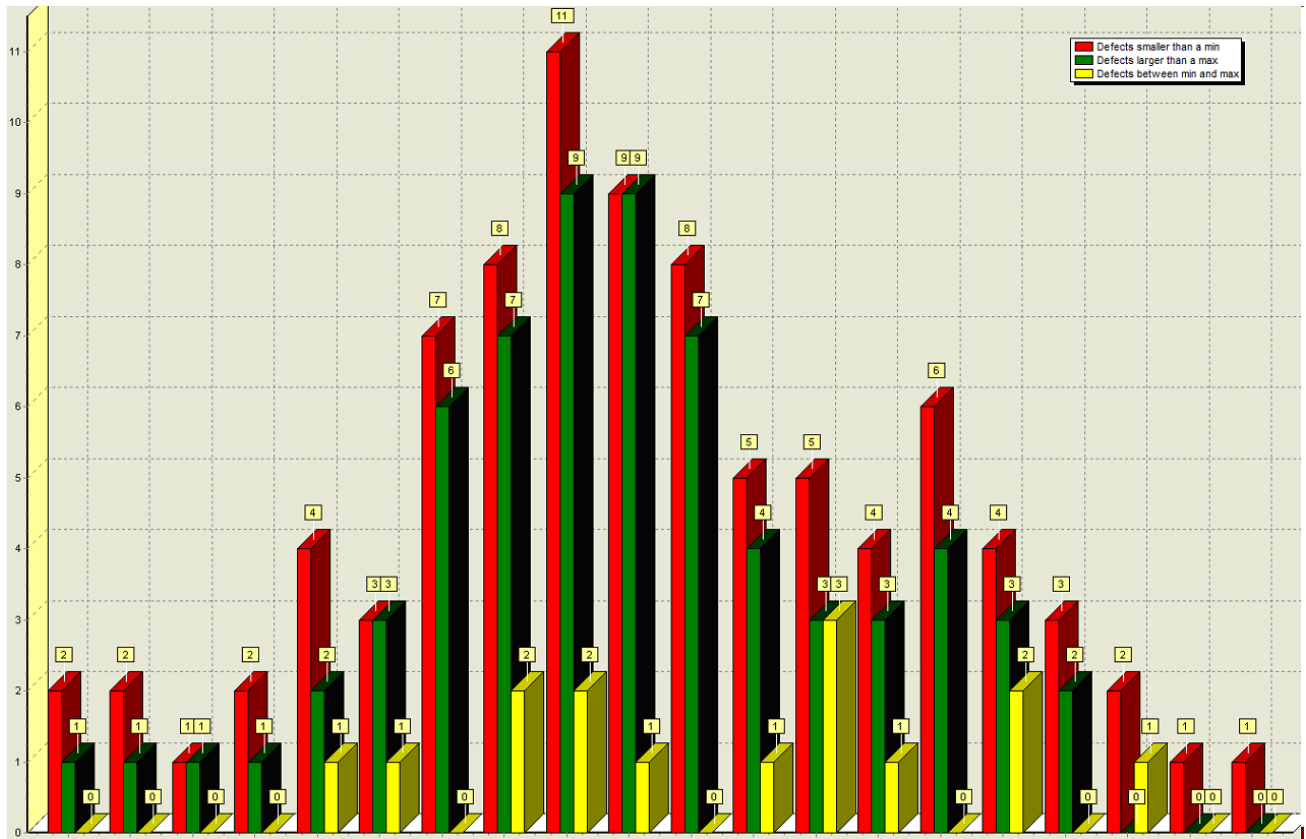


Fig. 7 – Histogram of the defect distribution by size in the layers

4.5 Test 5

The correctness of recognition for several types of defects. We generated a "virtual" crystal with 10 large defects (over $20\ \mu\text{m}$), 500 medium defects ($5\text{-}20\ \mu\text{m}$),

Table 1 – The results of testing *DefectGen-DefectMap* software

Test number	Generate			Recognize			Recognition degree, %
	Small ($< 5\ \mu\text{m}$)	average ($5\text{-}20\ \mu\text{m}$)	large ($> 20\ \mu\text{m}$)	Small ($< 5\ \mu\text{m}$)	average ($5\text{-}20\ \mu\text{m}$)	large ($> 20\ \mu\text{m}$)	
1	0	0	20	0	0	18	90
2	0	0	20	72	0	20	100
3	0	300	0	6	290	0	97
4	0	300	0	80	287	0	96
5	5000	500	10	4534 (91%)	475 (95%)	12 (120%)	

As is evident, this is an excellent method for assessing the quality of recognition programs used to measure defects in semiconductor crystals. Moreover, research with the *DefectGen-DefectMap* software showed high recognition fidelity for the right software configuration. Specifically, we found that the noise overlay primarily affects the quality of the recognition for small defects, but the use of noise filtering (Test 2) is effective in reducing the number of artifacts almost completely.

We did not find any programs analogous to the developed software described here in open-access literature, probably because similar programs are very application specific, expensive to create, and were developed by private companies to assist with the manufacturing of semiconductor crystals.

and 5000 small ones (smaller than $5\ \mu\text{m}$) without any noise. Analysis of the histogram shows that the application recognized 12 large defects, 475 mid-size defects, and 4534 small ones. The overall test results are shown in the table (Table 1).

5. CONCLUSIONS

From our experiments and validation testing, we conclude that our software package offers a wide range of opportunities for studying the structure of defects in semiconductor crystals. We have applied the software for processing the results of as-grown and thermally processed crystals of CdTe and CdZnTe, and found good reliability for measuring defects and their 3D distributions. It is clear that our software can be used to analyze the defect subsystems of any solid for which the internal structure can be presented in sequential layers of microphotographs. The possibility of obtaining three-dimensional images and for statistical analysis of the distribution of defects greatly simplifies the process of visualization and the evaluation of defect subsystems.

The ability to adjust the brightness, contrast, and use filtering and editing tools allows for higher accuracy in the object recognition.

For the first time, we have proposed and implemented a quantitative method of checking the accuracy of recognition software by generating and using a "virtual" crystal with predetermined parameters. The high accuracy of our *DefectMap* software in resolving the entire spectrum of growth defects was demonstrated.

Modification of the developed software allowed its usage to automate the analysis of the tracks of metal nanoparticles in colloidal solutions (nano-tracking), define their parameters, and obtain their statistical distribution according to diameters, colors, and dynamics of movement. This analysis demonstrates the feasi-

bility of using the developed software in the modes of micro-thermometry and micro-viscometry, i.e., in determining the local temperature and viscosity of the solution.

ACKNOWLEDGEMENTS

This work was performed under the project "Development of the software and hardware systems for nano- and microscopic parameters research in colloid solutions and solids" (0115U003240) with the financial support of Ministry of Education and Science of Ukraine. Two of us received partial support from U.S. Department of Energy NNSA Defense Nuclear Nonproliferation R&D.

REFERENCES

1. P.P. Jonker, R.P.W. Duin, D de Ridder, *Steel Grips* **1**(1), 20 (2003).
2. R.S. Sabeenian, M.E Paramasivam, P.M. Dinesh, *Intern. J. Comp. Appl.* **58**(11), 21 (2012).
3. C. Koch, K. Georgieva, V. Kasireddy, B. Akinci, P. Fieguth, *Adv. Eng. Inform.* **29**, 196 (2015).
4. E. Belas, M. Bugár, R. Grill, P. Horodyský, R. Fesh, J. Franc, P. Moravec, Z. Matěj, P. Höschl, *J. Electron. Mater.* **36**(8), 1025 (2007).
5. E. Belas, M. Bugar, R. Grill, J. Franc, P. Moravec, P. Hlidek, P. Höschl, *J. Electron. Mater.* **37**(9), 1212 (2008).
6. X. Zhang, Z. Zhao, P. Zhang, R. Ji, Q. Li, *J. Cryst. Growth* **311**(2), 286 (2009).
7. P. Fochuk, R. Grill, O. Kopach, A.E. Bolotnikov, E. Belas, M. Bugar, G. Camarda, W. Chan, Y. Cui, A. Hossain, K.H. Kim, I. Nakonechnyi, O. Panchuk, G. Yang, R.B. James, *IEEE T. Nucl. Sci.* **59**(2), 256 (2012).
8. G. Yang, A.E. Bolotnikov, P. M. Fochuk, Y. Cui, G.S. Camarda, A. Hossain, K. H. Kim, J. Horace, B. McCall, R. Gul, O.V. Kopach, S.U. Egarievwe, R.B. James, *J. Electron. Mater.* **38**, 1354 (2012).
9. K.H. Kim, J. Suh, A.E. Bolotnikov, P.M. Fochuk, O.V. Kopach, G.S. Camarda, Y. Cui, A. Hossain, G. Yang, J. Hong, R.B. James, *J. Cryst. Growth* **354**, 62 (2012).
10. L. D'yachenko, Yu. Tanasyuk, P. Fochuk, O. Panchuk, E. Minov, S. Ostapov, *Proceedings of the International Conference (CADSM-2009)*, 22 (Polyana-Svalyava: 2009).
11. S.F. Liu, F.L. Chen, Y.Y. Shi, S.M. Yu and C.S. Chang, *Proc. of the International Multi-Conference of Engineers and Computer Scientists (IMECS-2008)*, **2**, 19 (Hong Kong:2008).
12. Hong Qian, M.P. Sheetz, E.L. Elson, *Biophys. J.* **60**, 910 (1991).
13. T.L. Thu, P. Saveyn, H.D. Hoa, P. Van der Meerén, *Dairy J.* **18**, 1090 (2008).
14. V. Filipe, A. Hawe, W. Jiskoot, *Pharm. Res.* **28**, 1112 (2011).
15. R.D. Boyd, S.K. Pichaimuthu, A. Cuenat, *Colloid. Surf. A:* **387**(1), 35 (2011).
16. A. Chambolle, R.A. DeVore, N. Lee, B.J. Lucier, *IEEE T. Image Process* **7**, 319 (1998).
17. I.M. Johnstone, B.W. Silverman, *J. Royal Stat. Soc. B* **59**, 319 (1997).